Modern damage measurement of structural elements: Experiment, terrestrial laser scanning, and numerical studies

Masoud Mohammadi, Maria Rashidi [*], Mojtaba Gorji Azandariani [*], Vahid Mousavi, Yang Yu, Bijan Samali

Centre for Infrastructure Engineering, School of Engineering, Design and Built Environment, Western Sydney University, Penrith, NSW, Australia

ARTICLE INFO

ABSTRACT

In this modern era of civilization, with the rise of construction of structures worldwide, there has been an increasing demand for structural health monitoring and assessment, which ensures the durability and stability of structural life. Terrestrial laser scanner (TLS) is one of those state-of-the-art technologies which has simplified the structural survey and assessment. TLS can rapidly acquire millions of 3D data points from an entire structural surface with high precision in a short period of time, encompassing the physical position and geometrical details of the subjected object in the form of a digital replica known as Digital Twin (DT). A Digital Twin is the set of all digitally represented data, which can greatly benefit engineers in terms of generating a realistic 3D model of the structure and identifying the structural deformities such as deformations, displacements, surface anomalies/ir-regularities, etc. Despite the significant benefit of this technology, there has been limited research studies on its application and evaluation in terms of accuracy in structural monitoring and assessment. Therefore, this research paper aims to provide an experimental program that not only measures and quantifies the performance of TLS, but also evaluates its accuracy in comparison to other conventional single-point measurement equipment. In this regard, a simply supported structural beam has been considered as a structural object and subjected to monotonic loading. Meanwhile, the deformation of the beam has been captured using a few methods including TLS. The finding of this research showed that the TLS performed remarkable well with errors less than 2% compared to other accurate approaches of measurements.

1. Introduction

Infrastructures are the assets of the nation and need to be durable and healthy during their life span. In the surveys of engineering structures, one of the key objectives is to monitor the state of health of the structure during a lifetime. Infrastructures such as bridges are prone to deterioration before their age due to material aging, corrosive environment, overloading, and wear & tear process [1–3]. There have been several collapses and downfalls of the structure seen over past years due to inadequate adoption of the health monitoring system. The collapse of Taiwan's Nanfang'ao bridge on 1st October 2019 is an example of a catastrophic event caused by a lack of proper health monitoring and maintenance. Hence, such deterioration including deformations, and changes in their surface of the structural components, needs to be treated properly and systematically in regular terms and condition before any catastrophe and downfall of the structure occur. Structural

health assessment plays a crucial role in addressing such flaws and maintaining the well-being and durability of the infrastructures [4–7]. Presently, structure monitoring is mostly carried out based on traditional methods using visual inspection, manual assessment, and interpretation. However, it has several drawbacks such as being time-consuming, susceptible to error, labor-intensive, and subjective outcomes, etc. Apart from these, the difficult location of structures like bridges, dams, and tunnels makes structural monitoring based on traditional and manual inspection become harsh and unsafe [8–10].

The research problem highlighted in this study underscores the critical need for further research in the field of structural health assessment and monitoring, particularly through the application of Terrestrial Laser Scanning (TLS). While the study acknowledges the advancements and benefits of TLS in capturing three-dimensional point cloud data for structural assessments, it also reveals the limitations of traditional methods that are time-consuming, error-prone, labor-

* Corresponding authors.
E-mail addresses: m.rashidi@westernsydney.edu.au (M. Rashidi), m.gorjiazandariani@westernsydney.edu.au, gorji1365@yahoo.com (M.G. Azandariani).
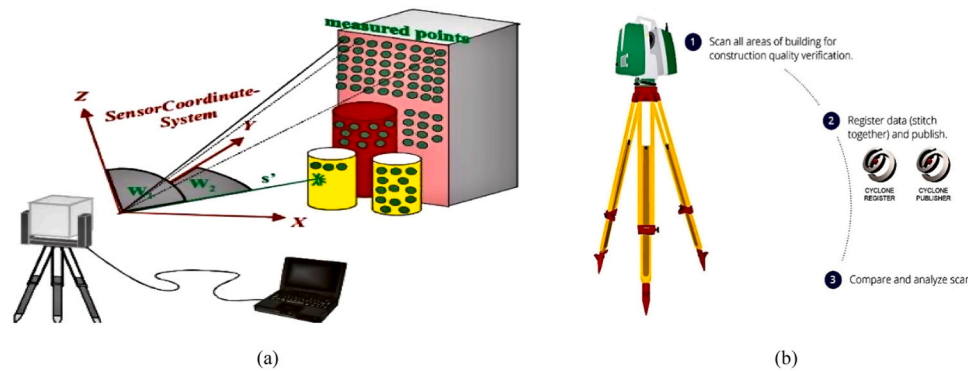
Fig. 1. (a) Working principle of TLS, and (b) Working flow diagram for TLS [13].

intensive, and subject to various challenges, especially when dealing with complex and inaccessible structures such as bridges, dams, and tunnels. In addition, catastrophic collapse of structures due to inadequate health monitoring and maintenance are stark examples of the potential consequences of ignoring infrastructure health. Given these challenges and the increasing importance of maintaining durable and healthy national assets, there is a compelling need for more comprehensive research in this field. Further investigations can delve into refining the TLS technology, developing more robust algorithms, and exploring its practical applicability on a broader range of structures. Such research can significantly contribute to enhancing the reliability and effectiveness of structural health assessments, ultimately ensuring the safety and longevity of critical infrastructures.

A modern technology of acquiring 3D position data of an entity or body surface rapidly and precisely through the advanced feature of contactless surveying to form a digital replica of an object is Terrestrial Laser Scanning (TLS), which overcomes traditional methods in terms of speed, accuracy, and range [8,11]. An introduction of TLS in engineering structural surveys and creation of Digital Twins (DT) using this technology, solve such shortcomings and ineffective structural assessments. TLS generates millions of 3D coordinate (x, y, and z) points of an object by sending and receiving laser beams and measuring the distance, horizontal angle, and vertical angle between the objects. Fig. 1(a) shows a typical principle of TLS for point cloud data acquisition. TLS obtains 3D- point cloud data acquisition of an entire object surface precisely which facilitates users to obtain a three-dimensional measurement, and accurate 3D-model creation. Apart from the physical coordinates of an object, the in-built RGB camera in the latest TLS unit can generate globular panoramic RGB (red, green, blue) images. These colorimetric RGB values will be allocated and mapped to a 3D point in the software through the matrix of the transformation. The point cloud data obtained immediately after scanning is registered in one coordinate system for further processing of data from which 3D modelling and quality inspection of structure can be accomplished [12]. Moreover, as data capture generally contains amount of redundant data and noises, the captured point cloud will also be subjected to a noise filtering process in the software through the post-processing procedures. Fig. 1(b) shows a basic working flow of the application of TLS for analysis purposes.

The major advantage of TLS over a traditional method is acquiring a complete set of data of the whole structure within a short period. TLS also facilitates surface inspection of inaccessible structural components feasible. The application of TLS and appropriate algorithms could considerably assist engineers in identifying structural issues such as displacement, undesirable deformation, surface anomalies, etc., from the acquired point cloud data, which are well-detailed in the literature review subsection.

1.1. Literature review

In the modern era of digitization and technology, TLS has been progressively adopted for surface anomaly detection, such as displacement and deformation monitoring [14,15]. One of the earliest attempts for monitoring structural deformation using a TLS was performed by Gordon [16] who carried out a test utilizing a TLS for accessing the sensitivity and vertical deformation due to external load as well as investigating the potential for metrology tasks that involve a remote examination. Nuttens et al. [17], Bitelli et al. [18], and Monserrat and Crosetto [19] obtained deformation values from point cloud data by making a comparison with Digital Elevation Model (DEM) for assessing the land deformation monitoring at various measurement epochs. In a similar strategy, Schäfer et al. [20] used TLS method for deformation monitoring of a hydropower station in different settings of liquid levels during the filling and emptying process. In another effort, Schneider [21] adopted the TLS application for determining the deformation of the water dam and the bending line of the television tower. Studied the practicability of TLS for monitoring the deformation of a large concrete dam. TLS has proven to be useful and reliable in monitoring long-term deformation. In this regard, TLS data has been used as a reference for both comparison and correlation analyses of the changes including deformations that occur over the structure's lifetime [22].

Zogg and Ingensand [23] monitored the deformation due to the load test on the Felsenau viaduct with the application of TLS and compared it with precise levelling data. The TLS Imager 5006 by Zoller + Froehlich was used to scan the bridge girder. Five reference targets were established in the test field, and these target points were scanned at super high resolution while another scanning was done at high resolution. The TLS-obtained 3D point cloud data were registered and filtered to obtain deformation values by comparing them with before and after loading data. For registering, all the 3D point cloud data are registered in one coordinate framework using cyclone software. The absolute error and Root Mean Square (RMS), which determines the registration quality for three registrations, varied from 0.5 to 0.6 mm. Geo-magic Qualify software was used to analyze deformation. Truong-Hong & Laefer [24] studied the application of TLS in bridge inspection involving geometric modelling and quality inspection. A point-surface-based approach was used to derive vertical bridge displacements that occurred due to dynamic load by calculating the discrepancy in the elevation of a bridge girder before and after loading. Yang et al. [25] experimented with determining health assessment of concrete structures like displacement, and other concrete structural effects using the finite element method (FEM) based on TLS. The specimen was performed with two cylinders at both ends for loading and the test setup. At first, the load of 4 KN was applied until the first crack was formed, and then the load was raised to 5 KN. The loading was kept on hold for 5 min, and loading was continued until the ultimate loading. The tested slab was inspected promptly, and load and deformation were measured using force sensors and displacement sensors. The triangular displacement sensors were kept in the center of the beam. TLS was utilized to acquire the point clouds of the beam at each loading step as the TLS gives the data in X, Y, and Z coordinates and contains noise, so they implemented
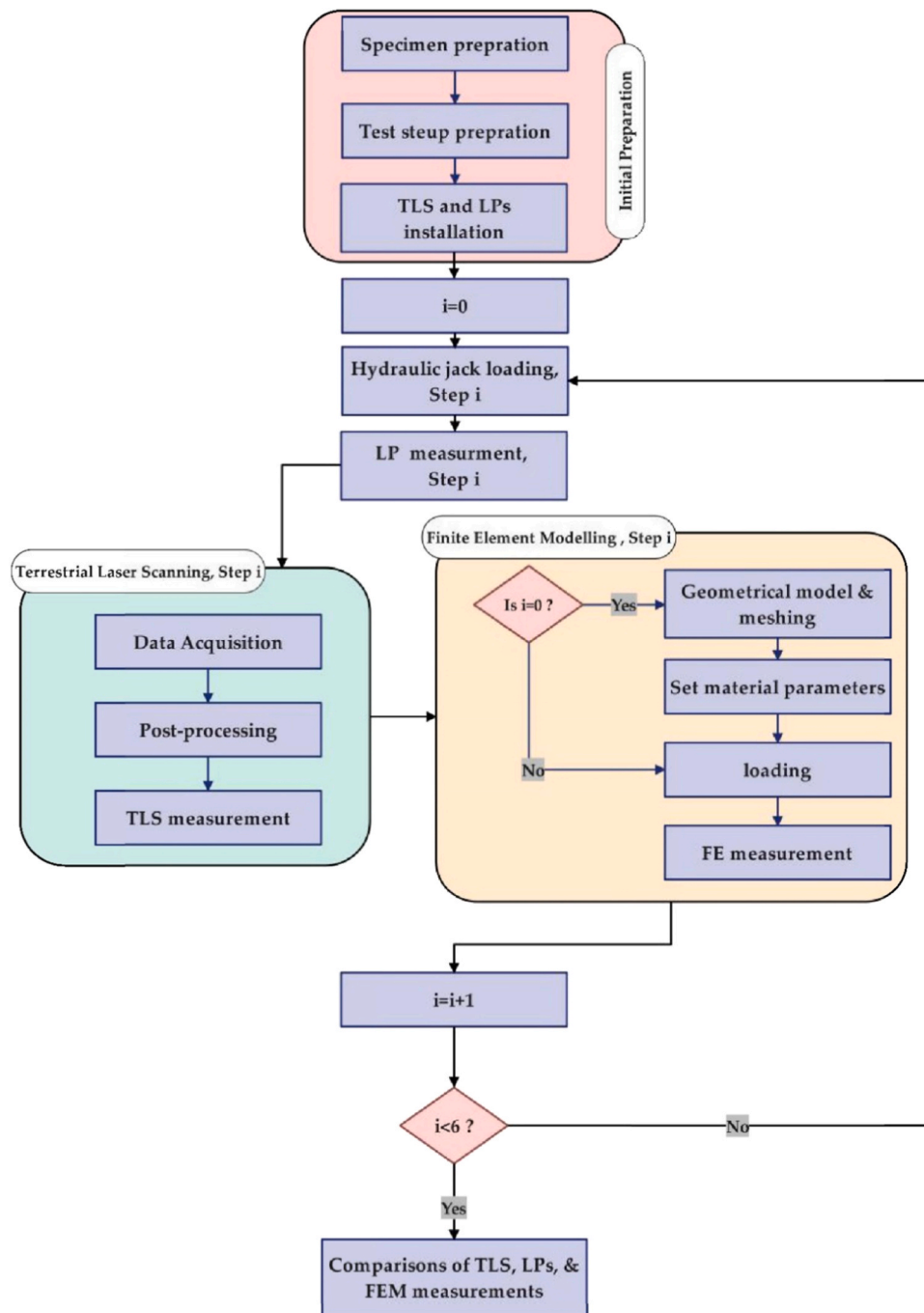
Fig. 2. The workflow of FEM model, TLS and LAB experiments comparison.

surface-based measurement analysis. The experiment mainly focused on determining the benefit of the 3D TLS for building convenient, intelligent, and efficient models that could be used to detect different structures like bridges, buildings, or subways. Yang et al. [26] applied laser scanning technology to model and observe the deformation of the arch structure. The experiment was carried out for 2 m spans of the arch with a thickness of 10 mm. The arch was subjected to monotonic loading with constant load speed and interval. Xu et al. [27] proposed a network method (NM) to analyze displacement effect in both terms of size and direction of a composite arched structure using TLS. The displacement map is extracted from point cloud data and a remapped network. This experiment used the finite element model (FEM) of concrete structures using TLS for optimizing the model through response surface methodology (RSM). The components used for the experiment were concrete

beams. Gawronek and Makuch [28] carried out a static load test at a railway bridge in Poland using TLS technology. The bridge was double-span continuous with a design span of 105.4 m. The experiment was carried out on a single bridge span by using loading models. This loading helped determine the dynamic change of structure that occurred due to uneven load during and after loading. A static load test was conducted on a span that facilitated the registration of the point cloud completely. Levelling and tachymetric measurements helped provide reference values to the values obtained from the TLS. At the end of the test, the maximum displacement found during static loading (−7.4 mm) was lesser than the optimal design deflection (−18.2 mm). Guo et al. [29] performed a comparative analysis to quantify the time and cost-efficiency of TLS based quality assessment. Structural columns were assessed with the application of TLS and it found that TLS application

had benefits in terms of time and cost. In another strategy, Mohammadi et al. [11] compared the quality of the TLS-based and Unmanned Aerial Vehicle (UAV) photogrammetry-based point clouds with as-designed drawings and as-is measurements on various bridge structural elements. This study revealed that TLS produced higher-quality data than UAV photogrammetry.

1.2. Objectives and aims of the research

The application of TLS provides all the required geometrical data necessary for structural damage assessment and quality inspection. The research proposes to investigate and evaluate the implementation of TLS in the measurement of displacement/deformation of the structural component. In this research, a structural beam was subjected to a monotonic loading scenario, and beam displacement was captured using TLS and compared with the 3D finite element model under the same loading protocol. The major objectives are as follows: **(i)** verify the reliability and applicability of point cloud data attained from TLS in structural assessment and health monitoring, **(ii)** identify and quantify the displacement and deformations of the proposed beam structure as part of structural damage assessment through the experimental test on a steel beam under real load, **(iii)** compare and validate the obtained result of TLS by the electromechanical measurement equipment, and numerical and analytical approaches.

2. Research methodology

According to the literature study, the practical and effective use of TLS in the field of structural assessment and health monitoring, has made this system an alternative for electromechanical measurement equipment and numerical and analytical approaches. This section details all of the steps required for collecting qualitative TLS data and elaborated the applicability of the proposed method for identifying and quantifying deformation and displacements in terms of structural monitoring and assessment. In this regard, an experimental case study was designed to assess the applicability of TLS in comparison to electromechanical measuring equipment such as Linear Potentiometers (LPs), which are normally used for the linear record of displacements. LPs are commonly used in structural assessments for displacement measurement, however, they can only record a point to which they are attached.

In this experimental program, three I-shaped steel beam specimens were subjected to a three-point bending test, and the deformation of the specimen from various points was taken using LPs and TLS. In these experiments, the specimens were subjected to a deformation-control loading protocol that included several displacement steps, and at each loading step, the LPs and TLS data were collected and compared. Another attempt has used the geometrical measurements of the specimens collected using TLS in the first step, prior to loading, to create a complete 3D model of the specimen to be used for Finint Element
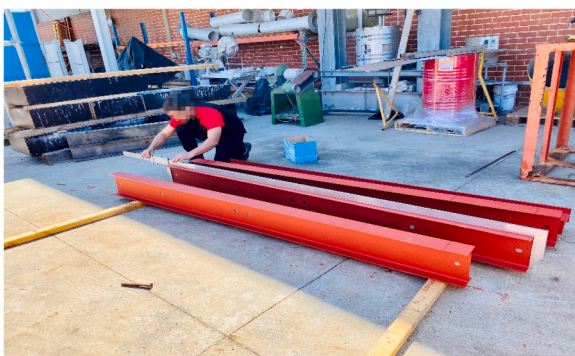

Fig. 3. Painting and measuring dimensions of specimens.

Modelling (FEM). The proposed workflow for TLS, and LP data collection, and FEM modelling are described in Fig. 2. The study's experimental workflow has been designed in six distinct loading steps, wherein the specimens are subjected to a displacement-controlled loading using a hydraulic jack and displacements at each loading step are measured using both LPs and TLS equipment. In the initial step (i.e $i = 0$), the 3D data acquired through TLS and it is utilized to generate a finite element model. This model is subsequently employed for beams' FEM simulation and comparison of specimen deformations. The loading procedure of specimens is conducted in a stepwise manner, with each step experiencing an increase in the load applied. Displacement information obtained from LPs and TLS is collected at every step, with a total of six progressive iterations. Ultimately, the measurements of deformation for LPs and TLS are analyzed and compared with the FEM's simulation outcomes. This comparison allows for a detailed tracking of the specimen's deformation, providing valuable insights into the physical properties of the specimens. The subsequent sections provide an explanation of the FEM model analysis and TLS-based deformation extraction.

2.1. Finite element modelling

The ABAQUS [30] software package was employed to generate a sample FEM model to simulate the beam deformations and compare the results with the conducted experiments with TLS and LPs. The FEM model enables the estimation of the displacement of all points on the surface of the object structure. Through an analysis of the stress and strain state of the deformed structure, it is possible to assess the displacements that have occurred as a result of load, strain, and stress. The type of material, size, shape, and applied forces can all contribute to various forms of deformation.

2.2. TLS-Based deformation extraction

The process of deformation extraction using TLS data analysis involves three primary steps, including data acquisition, post-processing, and displacement analysis for each epoch of point cloud data. The data collection is a pivotal step in generating a high-quality and large-scale point cloud. The effectiveness of the data for structural evaluation purposes is dependent upon the quantity and quality of the data collected [31]. Prior to obtaining point cloud data through laser scanning, it is essential to consider various parameters, such as but not limited to scan quality and resolution settings. It is necessary for operators to adjust these two parameters according to the minimum discernible object size in the point cloud data. Selecting the suitable values for these parameters is crucial to achieve high-quality results, minimize scanning time, and reduce the required time for post-processing of the point cloud data [32].

TLS point cloud data often comprises some outlier noise which refers to data points that exhibit substantial errors and deviate from the normal noise [33]. Moreover, the TLS scanning process usually captures objects that are not desired. As a result, it is necessary to implement a post-processing filtration stage in order to improve the quality of the acquired TLS data. The post-processing stage involves noise reduction and the elimination of non-beam features, such as equipment and tools, to enhance the accuracy and reliability of the point cloud data. Following the data collection and post-processing, the deformations of the beam in each epoch were extracted through the measurement of the vertical displacements at specific points along the beam. The obtained results are compared with those of the LPs and FEM simulation.

3. Experimental works

An experiment was conducted as part of a research methodology to investigate and evaluate the implementation of a TLS in the measurement of displacement of the structural component as a part of quality inspection. In this experiment, three simply supported structural beam,
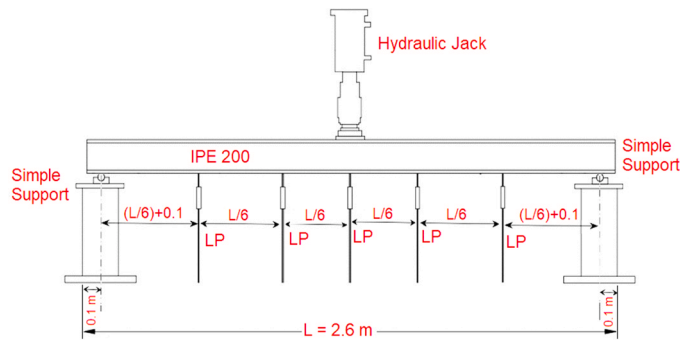
Fig. 4. Details of three-point Bending test.

i.e., IPE200 (d_b= 200, b_f=100 mm, t_f= 8.5 mm and t_w=5.6 mm) steel beam, was subjected under a monotonic load at mid-span in a bending test, and the beam performance under load was scanned at each load step by the TLS. The length of the beam is equal to 2.6 m. The occurring displacement and deformation were measured by processing the point cloud data obtained from TLS and compared with the electromechanical measurements and 3D finite element model under the same loading.

3.1. Preparation of specimens

The beam was sand dust and painted with rustproof paint in two layers of the coating as shown in Fig. 3, and left for drying before testing the specimen. Each dimension of the beam was measured with the help of a three meter-vernier caliper to have an accurate estimation of the beams dimensions.

3.2. Test Setup

An Electric universal testing machine was used to carry out a three-point bending test. The major benefit of a three-point bending test is the effortless preparation of test specimen and examination. The beam is placed over two support i.e. pinned support at one end and a roller support at another end. The loading is applied at a constant rate at the center of the beam with the help of hydraulic power controlled through-loading system/computer. The test setup for the beam in a 3-point bending test is shown in Fig. 4 and Fig. 5. The loading was stopped at each interval to allow for TLS scanning of the beam and then resumed for further loading. The loading was done beyond the failure of the steel beam to attain maximum deflection possible considering the lab safety and protocols.

3.3. Linear Potentiometer (LP's)

Linear potentiometer (LP's), also referred to as electromechanical measuring devices/sensor, converts the linear motion of a body coupled with LP's into an electric signal corresponding to the value of movement and is recorded in the linked system/computer. These devices quantify the real-time displacement of an object. For this experiment, five LP's are installed at L/6, L/3, L/2, 2 L/3, and 5 L/6 position of the steel beam and is attached to the bottom flange of the beam. After each interval of load, the values given by the LP's are recorded in the system. Fig. 4 demonstrates the location of five LPs installed in the bottom flange of the steel beam.

4. Measurement with TLS

The experiment described in Section 3 was based on the use of a TLS to scan, and record point clouds of simply supported beams while under a load applied at the beam's mid-span. The vertical displacement of each beam under each load was recorded at the five one-sixth points (L/6, L/3, L/2, 2 L/3, and 5 L/6) of the beam's 2.4 m span, L, by LVDTs (linear variable displacement transformers). The vertical displacements recorded by the LVDTs, which can be described as 'precise indicators of position' [34]), were used as baseline values. These baseline values would then be compared with vertical displacement values, as obtained from point clouds captured by TLS, of the same points on the same beams under the same loads. Additionally, the vertical displacement values of the physical beams, as obtained from both the LVDTs and the TLS, would be compared to values obtained from a 3D finite element model of the experiment.
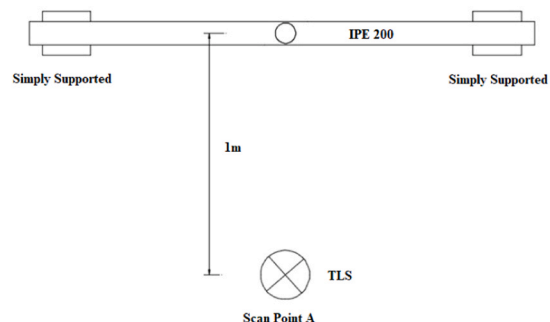

Fig. 6. Position of different Target points.

Fig. 5. Layout of TLS and test setup.

Fig. 7. Scanned image of the testing area and specimen from TLS.

4.1. TLS Instrumentation

The TLS device placement is kept in such a way that the device can completely scan the bottom flange portion of the beam, to were compared the displacement of the bottom flange with the displacement recorded from LP's. Moreover, the location of TLS is not fixed and critical as these points can be moved in any direction and placed in such a way there is no obstruction in the scanning process. Initially, the beam was scanned at zero loading conditions. And after that, scanning was done at different load-interval to attain maximum displacement. Five different target points were attached nearby the setup zone in a different location, as shown in Fig. 6 to ease the registration of the acquitted point cloud data.

As it was desired to have the TLS perform all of its scanning while levelled, the tripods used in the experiment were set up with their apex levelled through fine adjustment of the tripod legs' lengths. This condition was verified by an external spirit level, as the tripod apexes did not feature integrated spirit levels. This process of levelling the apexes of the tripods was done in the hope that the TLS would be able to be used interchangeably on top of each of its scan position supports (the tripods and steel universal columns (UCs)) without the need to adjust the TLS's tribrach between each movement of the TLS from one scan position to another. Unfortunately, it was found that the top flanges of the UCs did not provide surfaces level enough for the sensitivity of the TLS's in-built spirit level, and as the orientation of the UCs could not practically be fine-tuned, levelling of the TLS had to be performed via adjustment of the TLS's tribrach for each relocation between scan positions.

Once the TLS was levelled at a scan position, the location at which scan data was to be saved within the TLS's data storage drive was set via the TLS's integrated touch screen. The scanning process, and scan parameters affecting the density of the point cloud to be captured, could be initiated/modified via commands entered into the TLS's integrated touch screen; however, a laptop connected wirelessly to the TLS was also used to command the TLS through dedicated software. The laptop, with its mouse and keyboard, was the preferred option for commanding the TLS, and was particularly suited towards defining the frame of view over which the TLS was to perform its detailed scanning. On both the laptop, and the TLS's screen, it was possible to see the 360° panoramic colour

Fig. 8. Image of Z + F IMAGER® 5016.

images captured by the TLS's integrated camera of the experiment for immediate review. In addition, the time remaining to complete each scan, and the time remaining to complete the capture of each panorama, was communicated live on both the TLS's screen, and via the laptop. Fig. 7 shows a 360° view of the experiment area as captured by the TLS's integrated camera. The scanning is done from one central location near the loading setup of the beam, as shown in Fig. 7. Initially, the whole area was scanned at normal resolution with high-quality scan, and then finally from the first preview scan, the specimen section was selected and then finally scanned with super high resolution and premium quality. Such adoption saved the time of scan as scanning the whole area at higher resolution and premium quality would take a longer period for each scanning. As the specimen section was scanned at higher resolution and premium quality, the accuracy of the scan was not compromised and was relatively near 3 mm.

4.2. Specification of utilized TLS

The Z + F Imager®5016 has been utilized to carry out the test procedures. Table 1 provides technical information on Z + F Imager®5016

Table 1
Technical data of Z + F Imager®5016 TLS.

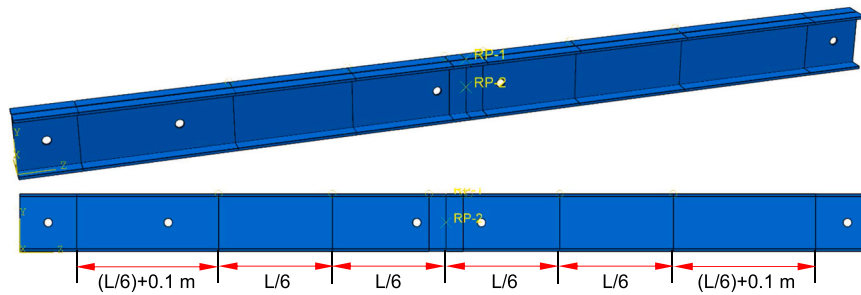| Manufacturer	Model	Imaging mechanism	working Principle	Data acquisition rate	Field of View (FOV)	Range	Resolution
Zoller+Fröhlich	IMAGER 5016	HDR panoramic	Phase measurement	Up to 2 million pixel/sec	360 × 320	> 360 m	Up to 0.8mm@10m

Fig. 9. The details and geometry of model.

TLS. The laser scanner unit is designed for a compact and light-weight model to make it more user friendly in handling and application (Fig. 8). With the advanced technology, the maximum range of this TLS is up to 360 m, thereby expanding its applicability and prospects at higher range applications. This scanner can capture one million points per second precisely. The field view of 360° × 320° reduces the number of scan locations and ensures great exposure of the scanned vicinity. The laser scanner is categorized as completely safe for the human eye and body and hence can be used in a public zone without any constraints. The integrated positioning system in the scanner enables registration automatically, even without any target points. This scanner is equipped with rapid scanning technology and takes just 3 and a half minutes approximately to capture a full HDR panorama view of 80 megapixels. The integrated LED spots with HDR camera allows user to capture images even in low light area. The storage capacity of the scanner is 128 GB and transferring of these data can be promptly done through connected Wi-Fi or secure digital card slot or ethernet cable.

4.3. Cloud compare software

Cloud compare is an advanced software capable of processing 3D point cloud data acquired from TLS. In this research work, the latest stable version 2.11.3 of cloud compare has been used for processing the point cloud data of the scanned beam. The software is capable of handling infinite scalar fields per point cloud and enables a user to visualize real field data. The segmentation option using a 2D polyline draw was used to segment, select beam section, and reduce noise from the entire point cloud data. From the pick point, option two points are selected to compute the corresponding distance between these two points.

5. Finite element modelling

In recent years, finite element modelling (FEM) has been widely used by various engineers and mathematicians in the field of engineering. The advantages of FEM are limitless and can be used to solve a different complex problem without any restriction. The modelling and simulation of the deformation of the I-shaped steel beam were carried out in ABAQUS [30] software. ABAQUS [30] software is widely adopted FEM software with powerful tools to solve a variety of complex problems with both linear and non-linear analysis [35,36].

5.1. Basic FEM equations

In this section, were delved into the fundamental equations used in standard displacement-based finite element analysis. The equilibrium equation, which is based on the virtual work principle, is expressed as follows [30]:

$$\int_V \sigma : \delta D dV = \int_S t^T . \delta v dS + \int_V f^T . \delta v dV \tag{1}$$

The left-hand side of Eq. (1) is substituted with the integral over the

reference volume of the virtual work rate per reference volume. This is defined by any conjugate pairing of stress and strain, and can be expressed as follows:

$$\int_{V^0} \tau^c : \delta\varepsilon dV^0 = \int_S t^T . \delta v dS + \int_V f^T . \delta v dV \tag{2}$$

where τ^c and ε are any conjugate pairing of material stress and strain measures. The particular choice of ε depends on the individual element.

The finite element interpolator can be written in general as:

$$u = N_N u^N \tag{3}$$

where N_N are interpolation functions that depend on some material coordinate system, u^N are nodal variables, and the summation convention is adopted for the uppercase subscripts and superscripts that indicate nodal variables.

The virtual field, δv, must be compatible with all kinematic constraints. Introducing the above interpolation constrains the displacement to have a certain spatial variation, so δv must also have the same spatial form:

$$u = N_N u^N \tag{3}$$

The continuum variational statement Eq. (2) is, thus, approximated by a variation over the finite set δv^N.

Now $\delta\varepsilon$ is the virtual rate of material strain associated with δv, and because it is a rate form, it must be linear in δv. Hence, the interpolation assumption gives as follows:

$$\delta\varepsilon = \beta_N \delta v^N \tag{4}$$

where β_N is a matrix that depends, in general, on the current position, x, of the material point being considered. The matrix β_N that defines the strain variation from the variations of the kinematic variables is derivable immediately from the interpolation functions once the particular strain measure to be used is defined.

Without loss of generality we can write $\beta_N = \beta_N (x, N_N)$, and with this notation the equilibrium equation is approximated as follows:

$$\delta v^N \int_{V^0} \beta_N : \tau^c dV^0 = \delta v^N \left[\int_S N_N^T . t dS + \int_V N_N^T . f dV \right] \tag{5}$$

Since the δv^N are independent variables, was can choose each one to be nonzero and all others zero in turn, to arrive at a system of nonlinear equilibrium equations:

$$\int_{V^0} \beta_N : \tau^c dV^0 = \int_S N_N^T . t dS + \int_V N_N^T . f dV \tag{6}$$

This system of equations forms the basis for the (standard) assumed displacement finite element analysis procedure and is of the form:

$$F^N (u^M) = 0 \tag{7}$$

The above equations are valid for static and dynamic analysis if the body force is assumed to contain the inertia contribution. In dynamic analysis, however, the inertia contribution is more commonly
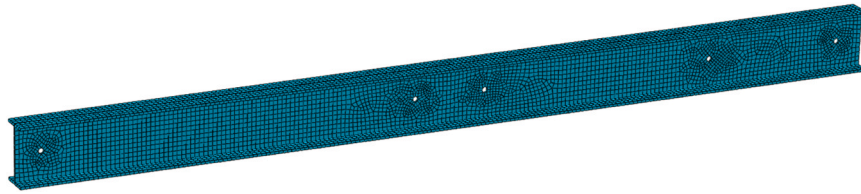
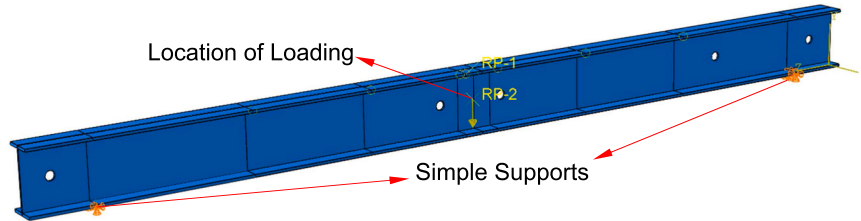**Fig. 10.** The meshing of the steel beam model.

Fig. 11. Boundary condition and loading of the steel beam model.

considered separately, leading to the equations as follows:

$$M^{NM}\ddot{u}^M F^N(u^M) = 0 \tag{8}$$

5.2. Geometrical modelling

The material properties and different geometry parameters are defined initially to model and carry out the analysis. The details of model geometry have been presented in Fig. 9. The beam is considered as a linear isotropic material for analysis purpose. The young's modulus of elasticity (*E*) for IPE 200 Steel Beam is taken as 193 GPa, whereas the Poisson's ratio has been considered as 0.3. The geometry of the model is 3D and the solid element is used for construction in the graphics module of the part. The geometry created in the assembly section is called and partitioned to increase the speed in the analysis and meshing of the model. Also, to collect the data at *L*/6, *L*/3, *L*/2, 2 *L*/3, and 5 *L*/6 positions according to the laboratory sample, the finite element model is partitioned according to Fig. 9.

5.3. Meshing

Meshing refers to the conversion of the whole body into a smaller division by defining mesh density and mesh shape. The meshing of the generated model is carried out to verify the position of node/element and decrease the error in solved results. The finer the mesh, the greater the degree of accuracy. However, the computing time will be immensely increasing with solving such fine mesh. Due to the partitioning of the model in the assembly module, it is possible to use C3D8R which is a general purpose linear brick element [37]. In this type of mesh, the element is in the form of regular eight nodes with high analysis power and appropriate accuracy. In the numerical analysis of this node, the reduced integral is used. Also, due to the regularity of the elements, the speed of analysis also increases. The dimensions used for meshing in this analysis are equal to 15×15 mm^2 according to the sensitivity analysis performed by Rousta et al. [38]. The meshing of the steel beam model is shown in Fig. 10.

5.4. Boundary condition and loading

The subsequent boundary condition for each support is defined (Fig. 11). Roller support at one end and pinned support at another end have been defined to make a simply supported beam. Roller support enables the beam to move in the x-direction while the y-direction is constrained. The loading condition is applied and expressed in the form
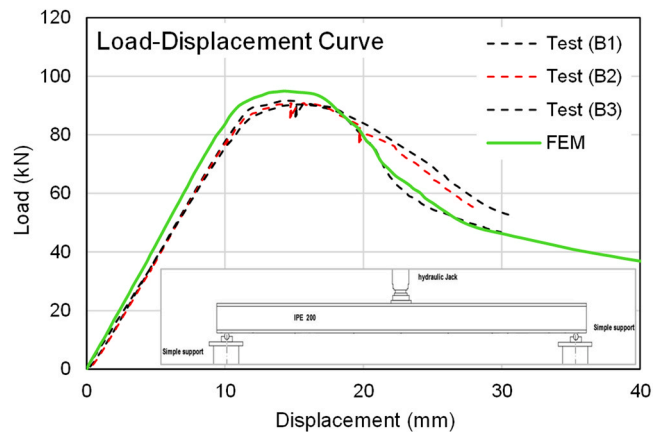

Fig. 12. Plot load vs displacement.

of initial displacement. The load case is applied at the center of the beam as a concentrated load. Finally, the model is solved using the defined analysis, and the results are obtained. These model results were compared with the numerical model and experimental data.

6. Result and discussion

In this section, the results of the study are presented and discussed with a primary focus on assessing the reliability of Terrestrial Laser Scanner (TLS) measurements. The TLS measurements are benchmarked against data obtained from LP measurements as the actual reference and FEM as a simulation approach. The time spent on laser scanning and capturing of test beams with TLS testing, while the rays were in a specific vertical displacement, was calculated by subtracting the loading pause time from the moment when the loading stopped, on a specific vertical displacement. The average total time spent on loading the rays and laser scanning is 4 h and 15 min, with 45 min of it attributed to laser scanning time. From the result of the three-point bending test on three specimens of IPE beam 200, a load vs. displacement graph has been plotted as shown in Fig. 12. The straight line in the graph indicates the zone of the elastic limit of the steel beam where the stress and strain are proportional to each other and experiences elastic deformation. And ahead of this elastic limit, the steel beam encounters plastic deformation and maximum stress and then finally fracture stress. The FEM is achieved with the help of ABAQUS [30] software. The curve of load-displacement

Table 2
Record data of the experiment, numerical, and TLS on test specimens.

| Specimen No.	Steps	Load (kN)	Deflection of Beam's Mid-span (mm)			$\frac{\delta_{Test}}{\delta_{FEM}}$	$\frac{\delta_{Test}}{\delta_{TLS}}$	$\frac{\delta_{TLS}}{\delta_{FEM}}$
			Test	FEM	TLS			
1	1	37.83	6.25	6.72	6.70	0.93	0.96	1.01
	2	38.11	6.40	6.87	6.65	0.93	0.94	1.03
	3	88.92	16.10	17.20	16.70	0.94	0.96	1.03
	4	86.20	16.12	17.41	16.72	0.93	0.96	1.04
	5	44.65	29.90	32.25	31.50	0.93	0.95	1.02
	6	41.09	29.89	32.14	31.49	0.93	0.95	1.02
2	1	33.76	5.05	5.52	5.39	0.93	0.93	1.02
	2	34.09	5.14	5.45	5.45	0.93	0.95	1.00
	3	77.74	10.39	11.15	10.94	0.93	0.95	1.02
	4	76.62	10.35	11.25	10.90	0.92	0.95	1.03
	5	88.53	15.01	16.07	15.55	0.93	0.96	1.03
	6	85.07	14.9	15.93	15.45	0.94	0.96	1.03
	7	81.44	19.94	21.27	20.49	0.94	0.97	1.04
	8	77.66	19.97	21.25	20.52	0.94	0.97	1.04
	9	50.85	30.03	31.82	30.58	0.94	0.98	1.04
	10	45.69	30.05	31.78	30.55	0.94	0.98	1.04
	11	33.90	45.81	48.39	46.36	0.95	0.99	1.04
3	1	30.49	4.84	5.20	5.07	0.93	0.96	1.03
	2	30.62	4.91	5.22	5.15	0.94	0.95	1.02
	3	72.05	9.97	10.58	10.20	0.94	0.98	1.04
	4	71.35	9.94	10.77	10.17	0.92	0.98	1.06
	5	89.49	15.02	15.89	15.25	0.95	0.98	1.04
	6	87.29	15.04	15.97	15.27	0.94	0.98	1.05
	7	80.20	19.97	21.08	20.20	0.95	0.99	1.04
	8	73.66	20.05	21.17	20.28	0.95	0.99	1.04
Mean						0.94	0.97	1.03
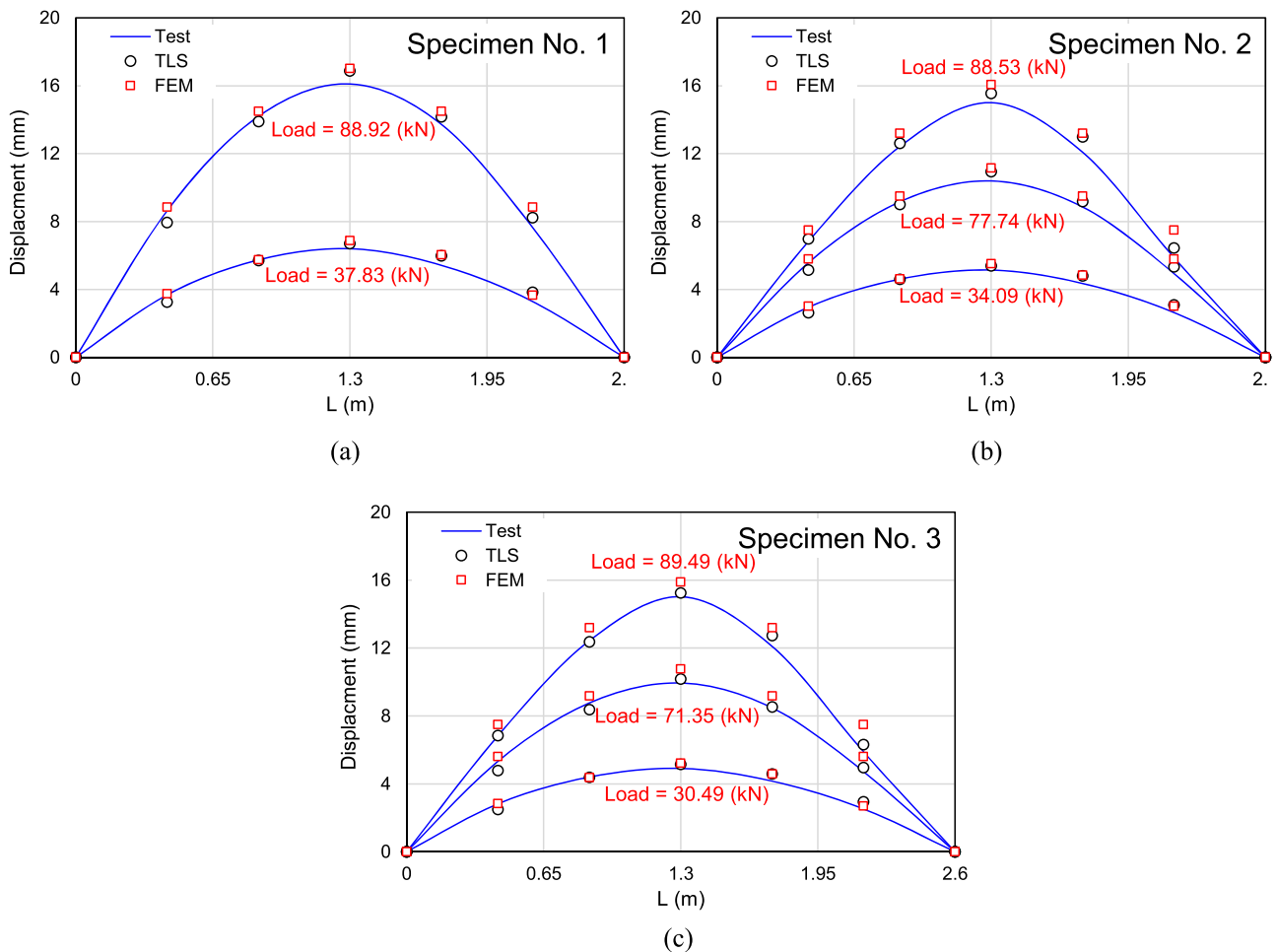
Fig. 13. The plot of displacement along the beam for the different loads: (a) Specimen No. 1, (b) Specimen No. 2, and (c) Specimen No. 3.
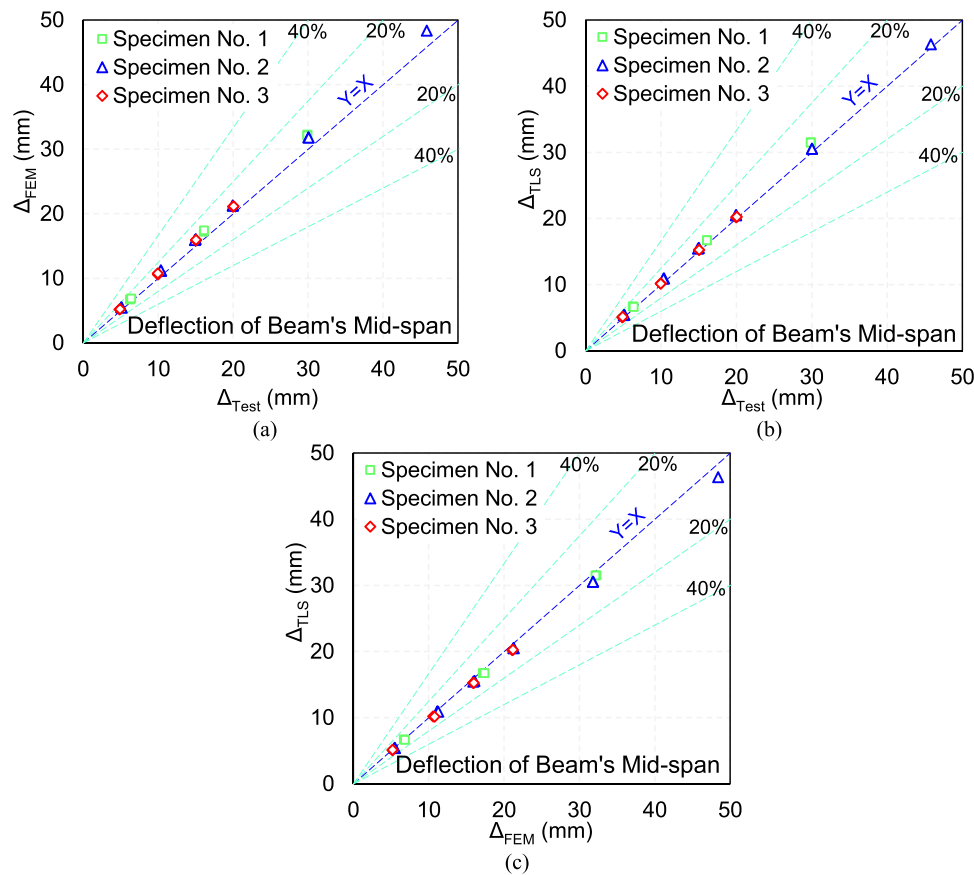
Fig. 14. Comparisons of record data of the experiment, numerical, and TLS: (a) Test vs. FEM, (b) Test vs. TLS, and (c) FEM vs. TLS.

obtained from numerical modelling corresponding to applied load is exhibited in Fig. 12.

The data of the photographed experiment has been included in this section. Table 2 is developed to present the beam displacement data results obtained from the experiment, numerical method, and laser scanning and compares them with each other. These columns indicate the vertical deflection of the test beam's mid-span, the laser scan, and numerical data, the test beams with the experiment's TLS. The vertical deflection of the test beam's mid-span at a particular time was calculated by subtracting the hydraulic testing ram's stroke, as soon as it first touched the top of the test beam, from the stroke of the hydraulic testing ram at the same particular time. The acquitted point cloud data is exported on 3D point cloud processing software i.e. Cloud Compare, and the results of computation of the distance between the bottom flange and reference line at a different stage of loading and the resultant displacement are tabulated in Table 2. The five LPs placed at mid-span from one end of the beam gave us the displacement values corresponding to the applied load for only those points in contact with LPs. The values of displacement obtained from LP's measurement corresponding to applied load are given in Table 2. In Table 2, the result obtained from the different approaches for the deflection value of the same beam has been compared, which provides a clear idea of efficiency, accuracy, and error of measurements. The result obtained from theoretical numerical formula and FEM validate the experimental result, whereas the result obtained from LP's is taken as reference for comparison of accuracy and error for TLS measurement. The summary of displacement values at x distance from the end for a beam corresponding to the applied load obtained from different methods is tabulated in Fig. 13. The plot of displacement values at 50 cm, 90 cm,130 cm, 170 cm, and 210 cm for Specimen No. 1 under the loads 37.83 kN and 88.92 kN obtained from the different approaches is shown in Fig. 13(a). Similarly, displacement values for Specimen No. 2 and 3 are shown in

Fig. 13(b) and (c). The measurement of maximum displacement value, which occurs at the center of the beam, through different approaches is summarized in Table 2. The results showed almost similar values of displacement of a beam from each method with slight variation. The percentage of error for the TLS measurement compared to other various approaches is tabulated in Table 2, which demonstrates that the error for measuring the smaller value of displacement is relatively higher, whereas with the increase in displacement value the error has been decreased and reached to 2%. Hence, a significant amount of displacement value can be accurately measured by TLS.

To assess the accuracy of TLS measurements, ratios between test vs. FEM, test vs. TLS, and FEM vs. TLS are provided. The ratio of the test values to the FEM predicted was determined and displayed in Fig. 14. The average ratio Δ_{Test} / Δ_{FEM}. is equal to 0.94. Similarly, Δ_{Test} / Δ_{TLS} denotes the ratio of the test values displacement to the TLS measurements, which is corresponding to 0.97. In addition, Δ_{TLS} / Δ_{FEM} is equal to 1.03, which signifies the ratio of the TLS measurement to the FEM predicted. The comparative analysis of the results indicates that TLS measurements generally align well with experimental values. The ratios for deflection of beam's mid-span are close to 1.00, suggesting a good agreement between TLS measurements and the experiments results. Overall, Fig. 14 demonstrate that the TLS provide a reliable estimation of the deflection for the analyzed specimens.

In the following, the deformed shape of the test samples, FEM and TLS are considered in order to compare and evaluate the results of the mentioned data recording approaches. Presentation of the results of the deformed shape of the finite element method is in the form of displacement contour. In the TLS method, a graphic image is used, which is a point cloud with high density. In the experimental method, the results are in the form of images recorded at every moment of loading. Fig. 15 shows the results of the deformed shape of the three-point bending test on the IPE 200 beam. Test data, FEM and TLS at
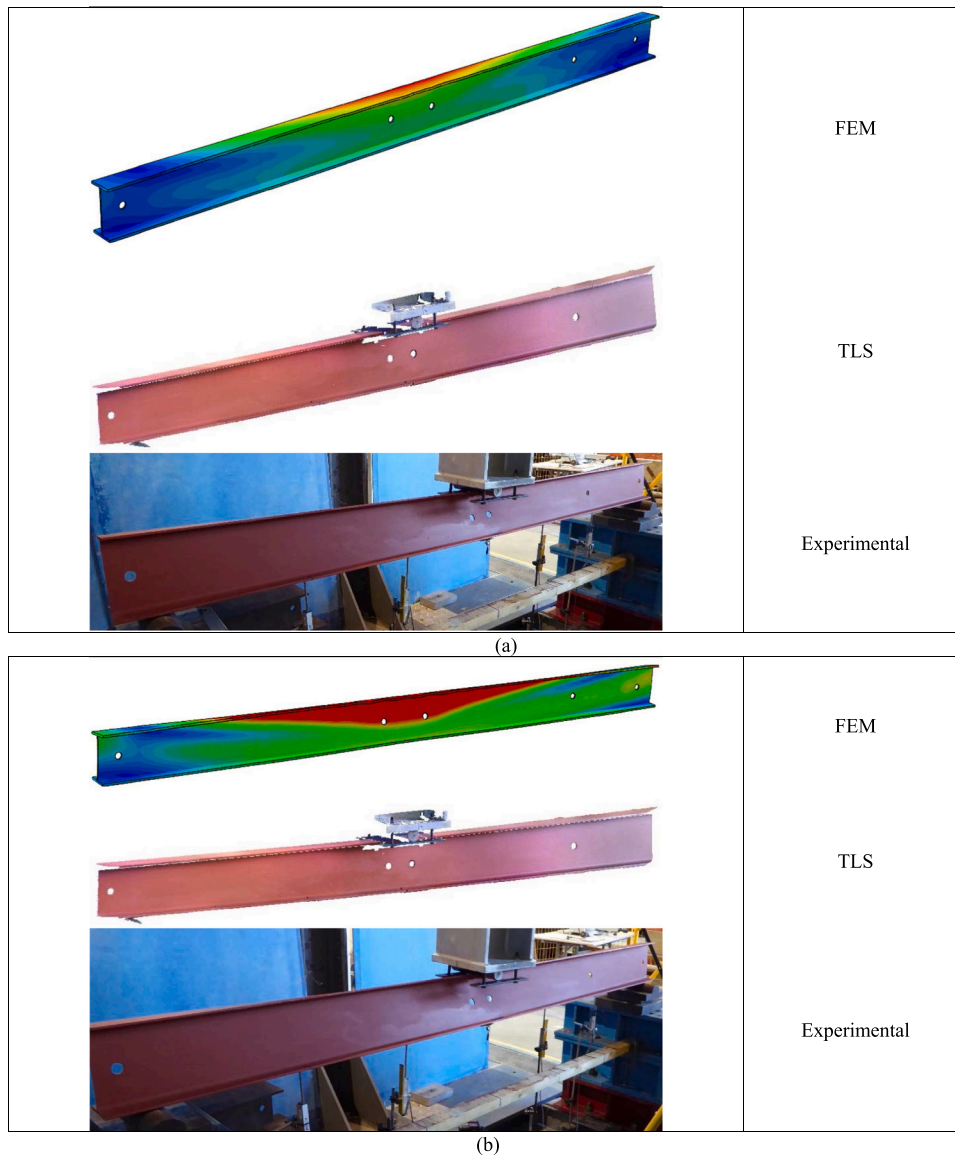
(a)

(b)

Fig. 15. Comparison of deformation shape of finite element method, TLS, and experimental specimens: (a) Specimen No. 1, and (b) Specimen No. 3.

specified loading are selected and included in this section. The laboratory results show that the deformed shape is in the form of torsion-bending buckling and in the out-of-plane direction. The comparison of the finite element method with the experimental results shows that the finite element model can present a clear deformed shape of the beam under three-point loading. Also, the comparison of the results taken by TLS with the deformed shape of the laboratory samples shows that the approach used in the TLS method and the point cloud results accurately recorded the deformation mode of the laboratory sample at different loading moments.

The discrepancy and variation in the results shows that the most probable reason is the consideration of different criteria and factors with certain limitations adopted in each approach which directly governs the error and accuracy of the measurement. The factors that could have largely affected the result are listed below:

(i) In the case of results from a TLS, the displacement values have been calculated without the consideration of holes which results in some percentage of error in comparison with actual experiment data and FEM. Slight geometric imperfection in the shape and size of the proposed beam might have imparted some errors

in the real test when compared with the hand calculation and FEM analysis where a beam with perfect geometry has been used.

(ii) Since the beam used for the experiment was old and rusted, the strength of steel obviously might have been decreased, and hence the experimental values differ from numerical and FEM modeling where standard properties of ideal steel beam have been used.

(iii) Due to lateral buckling and torsion of the steel beam, the bottom flange beam has twisted. As the displacement of the bottom flange has been considered, the LP's measured displacement of a single point is not capable of measuring such displacement.

(iv) Due to constrained space, the TLS device was placed almost 1 m apart from a beam and due to such proximity, errors were generated in capturing accurate point cloud data. The accuracy depends upon the selection of different features in TLS devices, such as resolution and quality of the scan. In this experiment, were used super high resolution with premium quality for each scan of a beam that has an accuracy of 3 mm. Therefore, the TLS technology can be used as a reliable alternative to the conventional measurement devices by capturing the whole specimen/ structural component, rather than measuring specific points.

7. Summary and conclusion

The objective of this study was to assess the accuracy and efficiency of Terrestrial Laser Scanning (TLS) as a method for measuring the displacement of a steel beam in comparison to traditional methods, namely finite element modeling (FEM) and experimental measurements. The study aimed to establish the reliability of TLS in capturing displacement data from the steel beam and to investigate any potential discrepancies and errors in comparison to the reference data obtained from FEM and experimental measurements. The research successfully achieved its objective by comparing the displacement values obtained from these different approaches, revealing that TLS measurements are in good agreement with both FEM and experimental results, particularly for larger displacement values. The scanner successfully measured different displacement values of the beam ranging from 1 mm to 30 mm at different load intervals. The findings show that the device was not able to detect smaller displacement values and had a greater error, whereas, in the case of larger displacement values, the device performed remarkably well and gave almost accurate values with an error of almost 2–4% compared with another approach of measurement. The discrepancies among different approaches is the result of different factors considered during the adoption of each method. In a numerical approach, the effect of lateral torsion and buckling effect was considered, whereas LP's measurement is only capable of measuring a particular point deflection to which it is attached. However, the TLS device can scan every single point and hence can define and measure each point's deflection and deformation. The accuracy of the TLS device mainly depends upon the resolution and quality of the scan. The higher the resolution and quality, the higher the accuracy. However, with such a higher configuration, the processing time and the corresponding data size become enormously superior. The study also identified specific factors that may contribute to discrepancies, including the geometric imperfections of the beam, the aging and rusting of the material, the complex deformation modes of the beam, and the proximity of the TLS device during scanning. In summary, the research demonstrated that TLS can accurately measure significant displacement values and provides valuable insights into the deformation modes of the steel beam, albeit with some limitations and potential sources of error that need to be considered in its application.

After successfully analyzing the results derived from TLS and comparing it with two other approaches of measurement, it can be concluded that TLS is an effective and accurate method for measurement of noticeable displacements and can be recommend for health monitoring of structures. However, the instrumentation cost of TLS and software for processing data is considered very high. Therefore, the applicability of TLS is recommended for larger projects such as bridges, dams, high rise buildings and railways.

Declaration of Competing Interest

The authors declare that they have no known competing financial interests or personal relationships that could have appeared to influence the work reported in this paper.

Acknowledgements

The authors extend their appreciation for the dedicated efforts of Pawan Regmi, Ankit Bhattarai, and Joshua Taylor.

References

[1] Laing R. Built heritage modelling and visualisation: The potential to engage with issues of heritage value and wider participation. Dev Built Environ 2020;4:100017. https://doi.org/10.1016/j.dibe.2020.100017.

[2] Cui L, Zhou L, Xie Q, Liu J, Han B, Zhang T, et al. Direct generation of finite element mesh using 3D laser point cloud. Structures 2023;47:1579–94. https://doi.org/10.1016/J.ISTRUC.2022.12.010.

[3] Kassotakis N, Sarhosis V. Employing non-contact sensing techniques for improving efficiency and automation in numerical modelling of existing masonry structures: a critical literature review. Structures 2021;32:1777–97. https://doi.org/10.1016/J.ISTRUC.2021.03.111.

[4] Mohammadi M, Rashidi M, Yu Y, Samali B. Integration of TLS-derived Bridge Information Modeling (BrIM) with a Decision Support System (DSS) for digital twinning and asset management of bridge infrastructures. Comput Ind 2023;147:103881. https://doi.org/10.1016/J.COMPIND.2023.103881.

[5] Zhang D, Liu TQ, Li S, Luo H, Ding G, Su Z, et al. Three-dimensional laser scanning for large-scale as-built surveying of 2022 Beijing winter olympic speed skating stadium: a case study. J Build Eng 2022;59:105075. https://doi.org/10.1016/J.JOBE.2022.105075.

[6] Otero R, Lagüela S, Cabaleiro M, Sousa HS, Arias P. Semi-automatic 3D frame modelling of wooden trusses using indoor point clouds. Structures 2023;47:1743–53. https://doi.org/10.1016/J.ISTRUC.2022.11.122.

[7] Safa M, Shahi A, Nahangi M, Haas C, Noori H. Automating measurement process to improve quality management for piping fabrication. Structures 2015;3:71–80. https://doi.org/10.1016/J.ISTRUC.2015.03.003.

[8] Rashidi M, Mohammadi M, Sadeghlou Kivi S, Abdolvand MM, Truong-Hong L, Samali B. A decade of modern bridge monitoring using terrestrial laser scanning: review and future directions. Remote Sens 2020;12:3796. https://doi.org/10.3390/rs12223796.

[9] Sacks R, Girolami M, Brilakis I. Building information modelling, artificial intelligence and construction tech. Dev Built Environ 2020;4:100011. https://doi.org/10.1016/J.DIBE.2020.100011.

[10] Gimenez L, Hippolyte JL, Robert S, Suard F, Zreik K. Review: reconstruction of 3D building information models from 2D scanned plans. J Build Eng 2015;2:24–35. https://doi.org/10.1016/J.JOBE.2015.04.002.

[11] Mohammadi M, Rashidi M, Mousavi V, Karami A, Yu Y, Samali B. Quality evaluation of digital twins generated based on uav photogrammetry and tls: Bridge case study. Remote Sens 2021;13:3499. https://doi.org/10.3390/rs13173499.

[12] Mohammadi M, Rashidi M, Mousavi V, Yu Y, Samali B. Application of TLS method in digitization of bridge infrastructures: a path to BrIM development. Remote Sens 2022;14:1148. https://doi.org/10.3390/rs14051148.

[13] Vosselman G, Maas H-G. Airborne and Terrestrial Laser Scanning. 1st ed.,, vol. 1. CRC Press; 2010.

[14] Sacks R, Girolami M, Brilakis I. Building Information Modelling, Artificial Intelligence and Construction Tech. Dev Built Environ 2020;4:100011. https://doi.org/10.1016/j.dibe.2020.100011.

[15] Luo H, Lin L, Chen K, Antwi-Afari MF, Chen L. Digital technology for quality management in construction: a review and future research directions. Dev Built Environ 2022;12:100087. https://doi.org/10.1016/J.DIBE.2022.100087.

[16] Gordon S., Lichti D., Franke J., Stewart M. Measurement of Structural Deformation using Terrestrial Laser Scanners. Gordon, S., Lichti, D., Franke, J., Stewart, M. (2004, June). Meas. Struct. Deform. using Terr. laser scanners. Proc. 1st FIG Int. Symp. Eng. Surv. Constr. Work. Struct. Engi, vol. 28, Nothingham, UK: 2004, p. 876–84.

[17] Nuttens T, De Wulf A, Deruyter G, Stal C, De Backer H, Schotte K. Application of laser scanning for deformation measurements: a comparison between different types of scanning instruments. Proc FIG Work Week 2012.

[18] Bitelli G, Dubbini M, Zanutta A. Terrestrial laser scanning and digital photogrammetry techniques to monitor landslide bodies. Int Arch Photo Remote Sens Spat Inf Sci 2004;35:246–51.

[19] Monserrat O, Crosetto M. Deformation measurement using terrestrial laser scanning data and least squares 3D surface matching. ISPRS J Photo Remote Sens 2008;63:142–54. https://doi.org/10.1016/j.isprsjprs.2007.07.008.

[20] Schäfer T., Weber T., Kyrinovic P., Zámecniková M. Deformation measurement using terrestrial laser scanning at the hydropower station of Gabcikovo. INGEO 2004 FIG Reg. Cent. East. Eur. Conf. Eng. Surv. Bratislava, Slovakia, 2004.

[21] Schneider D. Terrestrial laser scanning for area based deformation analysis of towers and water dams. Proc. 3rd IAG/12th FIG Symp., Baden, Austria, May, 2006, p. 22–4.

[22] Yang H, Xu X. Intelligent crack extraction based on terrestrial laser scanning measurement. Meas Control (U Kingd) 2020;53:416–26. https://doi.org/10.1177/0020294019877490.

[23] Zogg H-M, Ingensand H. Terrestrial laser scanning for deformation monitoring: Load tests on the Felsenau Viaduct (CH). Int Arch Photo Remote Sens Spat Inf Sci 2008;37:555–62.

[24] Truong-Hong L., Laefer D.F. Application of terrestrial laser scanner in bridge inspection: review and an opportunity. 37th IABSE Symp. Eng. Progress, Nat. People, Madrid, Spain, 3–5 Sept. 2014, International Association for Bridge and Structural Engineering (IABSE); 2014.

[25] Yang H, Xu X, Neumann I. Deformation behavior analysis of composite structures under monotonic loads based on terrestrial laser scanning technology. Compos Struct 2018;183:594–9. https://doi.org/10.1016/J.COMPSTRUCT.2017.07.011.

[26] Yang H, Omidalizarandi M, Xu X, Neumann I. Terrestrial laser scanning technology for deformation monitoring and surface modeling of arch structures. Compos Struct 2017;169:173–9. https://doi.org/10.1016/j.compstruct.2016.10.095.

[27] Xu X, Yang H, Neumann I. Monotonic loads experiment for investigation of composite structure based on terrestrial laser scanner measurement. Compos Struct 2018;183:563–7. https://doi.org/10.1016/j.compstruct.2017.07.001.

[28] Gawronek P, Makuch M. TLS measurement during static load testing of a railway bridge. ISPRS Int J Geo-Inf 2019;8:44. https://doi.org/10.3390/ijgi8010044.

[29] Guo J, Yuan L, Wang Q. Time and cost analysis of geometric quality assessment of structural columns based on 3D terrestrial laser scanning. Autom Constr 2020;110:103014. https://doi.org/10.1016/j.autcon.2019.103014.

[30] ABAQUS-6.14. Standard User's Manual. Hibbitt, Karlsson and Sorensen, Inc; 2014.

[31] Song M, Shen Z, Tang P. Data quality-oriented 3D laser scan planning. Constr Res Congr 2014 Constr a Glob Netw 2014:984–93.

[32] Dai F, Rashidi A, Brilakis I, Vela P. Comparison of image-based and time-of-flight-based technologies for three-dimensional reconstruction of infrastructure. J Constr Eng Manag 2013;139:69–79. https://doi.org/10.1061/(asce)co.1943-7862.0000565.

[33] Van Genechten B. Theory and Practice on Terrestrial Laser Scanning: Training Material Based on Practical Applications. Valencia, Spain: Universidad Politecnica de Valencia Editorial; 2008.

[34] Kedzierski M, Fryskowska A. Methods of laser scanning point clouds integration in precise 3D building modelling. Meas J Int Meas Confed 2015;74:221–32. https://doi.org/10.1016/j.measurement.2015.07.015.

[35] Firouzianhaij A, Gorji Azandariani M, Usefi N, Samali B. Performance of baseplate connections in CFS storage rack systems: an experimental, numerical and theoretical study. J Constr Steel Res 2022;196:107421. https://doi.org/10.1016/j.jcsr.2022.107421.

[36] Gorji Azandariani M, Rousta AM, Mohammadi M, Rashidi M, Abdolmaleki H. Numerical and analytical study of ultimate capacity of steel plate shear walls with partial plate-column connection (SPSW-PC). Structures 2021;33:3066–80. https://doi.org/10.1016/j.istruc.2021.06.046.

[37] Gorji Azandariani M, Gholhaki M, Kafi MA, Zirakian T, Khan A, Abdolmaleki H, et al. Investigation of performance of steel plate shear walls with partial plate-column connection (SPSW-PC). Steel Compos Struct 2021;39:109–23. https://doi.org/10.12989/scs.2021.39.1.109.

[38] Rousta AM, Gorji Azandariani M, Safaei Ardakani MA, Shoja S. Cyclic behavior of an energy dissipation system with the vertical steel panel flexural-yielding dampers. Structures 2022;45:629–44. https://doi.org/10.1016/j.istruc.2022.09.047.